A reduced resistive wall mode kinetic stability model for disruption forecasting

J. W. Berkery, S. A. Sabbagh, R. E. Bell, S. P. Gerhardt, and B. P. LeBlanc

Citation: Physics of Plasmas **24**, 056103 (2017); doi: 10.1063/1.4977464
View online: http://dx.doi.org/10.1063/1.4977464
View Table of Contents: http://aip.scitation.org/toc/php/24/5
Published by the American Institute of Physics

A reduced resistive wall mode kinetic stability model for disruption forecasting

J. W. Berkery,[1,a),b)] S. A. Sabbagh,[1] R. E. Bell,[2] S. P. Gerhardt,[2] and B. P. LeBlanc[2]
[1]*Department of Applied Physics and Applied Mathematics, Columbia University, New York, New York 10027, USA*
[2]*Princeton Plasma Physics Laboratory, Princeton University, Princeton, New Jersey 08543, USA*

(Received 17 November 2016; accepted 12 January 2017; published online 27 February 2017)

Kinetic modification of ideal stability theory from stabilizing resonances of mode-particle interaction has had success in explaining resistive wall mode (RWM) stability limits in tokamaks. With the goal of real-time stability forecasting, a reduced kinetic stability model has been implemented in the new Disruption Event Characterization and Forecasting (DECAF) code, which has been written to analyze disruptions in tokamaks. The reduced model incorporates parameterized models for ideal limits on β, a ratio of plasma pressure to magnetic pressure, which are shown to be in good agreement with DCON code calculations. Increased β between these ideal limits causes a shift in the unstable region of δW_K space, where δW_K is the change in potential energy due to kinetic effects that is solved for by the reduced model, such that it is possible for plasmas to be unstable at intermediate β but stable at higher β, which is sometimes observed experimentally. Gaussian functions for δW_K are defined as functions of $E \times B$ frequency and collisionality, with parameters reflecting the experience of the National Spherical Torus Experiment (NSTX). The reduced model was tested on a database of discharges from NSTX and experimentally stable and unstable discharges were separated noticeably on a stability map in $E \times$ B frequency, collisionality space. The reduced model failed to predict an unstable RWM in only 15.6% of cases with an experimentally unstable RWM and performed well on predicting stability for experimentally stable discharges as well. *Published by AIP Publishing.* [http://dx.doi.org/10.1063/1.4977464]

I. INTRODUCTION

In ideal magnetohydrodynamic theory, a fusion plasma is by definition stable with a normalized ratio of plasma stored energy to magnetic confining field energy up to a value of $\beta_N^{no-wall}$. The plasma is theoretically unstable above this "no-wall" beta limit to kink-ballooning modes when no wall is present, or the resistive wall mode (RWM) when a wall is present (Fig. 1). The RWM grows on the slower time scale of the penetration of magnetic perturbations through the wall, τ_w (typically milliseconds), but it is still fast compared with the duration of the plasma shot (typically seconds). Therefore it is necessary to stabilize this mode for continuous operation of tokamak fusion devices.

A new and advanced approach for unstable RWM avoidance is to use real-time physics-based models for early warning of approaching marginal RWM stability. Unstable RWM detection based on an experimentally measured exponentially growing magnetic signal is useful for characterizing the timing of the RWM and its place in the chain of events leading to disruption of the plasma current, but it can potentially come too late to take corrective action and to steadily maintain key plasma parameters such as the stored energy. Some examples of possible early warnings are the use of active MHD spectroscopy,[1,2] or the mismatch between the observer of an RWM state-space controller[3] and measured signals. Another method, which is described in detail presently, is to examine when the plasma toroidal rotation profile falls into a weaker RWM stability region based upon kinetic stability theory.[4–11] The recent success of kinetic modification to ideal theory, which contains broad stabilizing resonances via mode-particle interaction, in describing experimental RWM stability limits gives confidence in this approach. This approach will enable, for the first time, an unstable growing RWM to be *anticipated*, rather than being controlled after it becomes unstable. In all of these cases, one might then use a plasma rotation control system[12] to avoid these unfavorable profiles, while still having active control of the RWM.[13] Anticipation of the instability condition also potentially allows an active mode

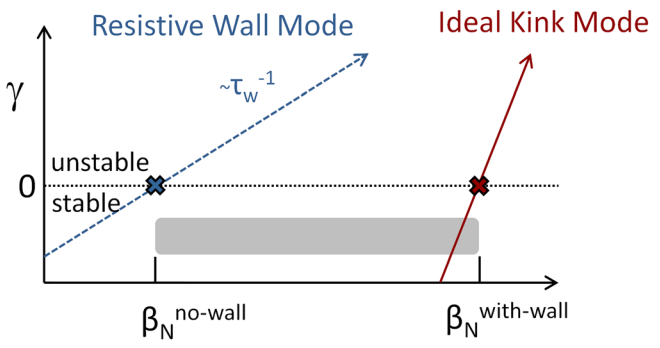

FIG. 1. Theoretical growth rates vs. β_N for the resistive wall mode and ideal kink. The grey area is where the resistive wall mode can be passively stabilized by kinetic effects.

Note: Paper YI2 5, Bull. Am. Phys. Soc. **61**, 407 (2016).
[a)]Invited speaker.
[b)]Electronic mail: jberkery@pppl.gov

control system to remain in a low-power state until needed, desirable for ITER and future devices.

In the present work we utilize the new Disruption Event Characterization and Forecasting (DECAF) code, which has been written for the general purposes of characterization of the chains of events which most often lead to disruption of plasmas and providing forecasts which integrate with a disruption avoidance system in multiple devices. The reduced kinetic stability model described here has been implemented within the framework of the DECAF code, with the ultimate goal of real-time operation in the NSTX-U[14] tokamak. Presently, the model is tested off-line on data from National Spherical Torus Experiment (NSTX),[15] the predecessor to NSTX-U. The model described here is "reduced" because the complexity of the kinetic stability theory and the present codes to calculate it are too large to run in real-time. That said, any reduced model still needs to be able to provide an accurate description of the full physics model over the operational space of the device to which it is being applied.

This paper is arranged as follows. First, in Section II, the expression for the growth rate of the RWM is described in detail. This is followed by specific attention to expressions for the ideal fluid terms which are necessary in Sections III and IV. Without yet defining the reduced kinetic term, the general behavior of the model in kinetic stability space is examined in Section V. In Section VI, the reduced kinetic model is described, implemented, and finally in Section VII, compared with experimental data to determine its effectiveness.

II. RWM STABILITY

The stability of plasmas to RWMs has been explained in multiple devices by employing calculations of kinetic effects,[2,8–11,16] with codes such as MISK.[5] MISK solves for the growth rate and real frequency (γ and ω_r) of the RWM through a dispersion relation dependent on the change in potential energy due to the perturbed kinetic pressure δW_K

$$(\gamma - i\omega_r)\tau_w = -\frac{\delta W_\infty + \delta W_K}{\delta W_b + \delta W_K}. \quad (1)$$

Note that the growth rate is normalized by the wall time and the units of the δW terms are arbitrary, as long as they are consistent. The fluid terms, δW_∞ and δW_b, represent the change in potential energy due to the mode when calculated without and with a wall, respectively. δW_K is calculated using the perturbed distribution function from the drift kinetic equation, and the solution involves a frequency resonance fraction $\lambda \sim (\omega_D + \omega_b - i\nu + \omega_E)^{-1}$, where ω_E, the $E \times B$ frequency, scales with the plasma rotation, which can be in resonance with the precession (ω_D) and bounce (ω_b) motions of the particles[9] and is effected by the particle collisionality[17] (ν).

We now turn to considering each of the δW terms, starting with the ideal fluid terms.

III. IDEAL NO-WALL LIMIT

A parameterization for the fluid no-wall β limit, which depends on parameters that can be measured or modelled in real-time (plasma internal inductance (l_i), pressure peaking ($p_0/\langle p\rangle$), and aspect ratio (A)), has been recently computed for NSTX.[16] Figure 2 shows that the so-called composite model does a good job predicting the no-wall limit calculated by the DCON stability code[18] for some of the first high-beta discharges in NSTX-U, the upgrade to NSTX.[14] This is despite the fact that the model was developed in the range of $l_i < 0.64$ and $p_0/\langle p\rangle < 2.25$, while the early NSTX-U discharges are above both of those ranges at high beta. The aspect ratio scaling ($\beta_{N,\text{no-wall}}^{n=1}$ decreases with increasing A[16,19]) corrects the difference between previous NSTX

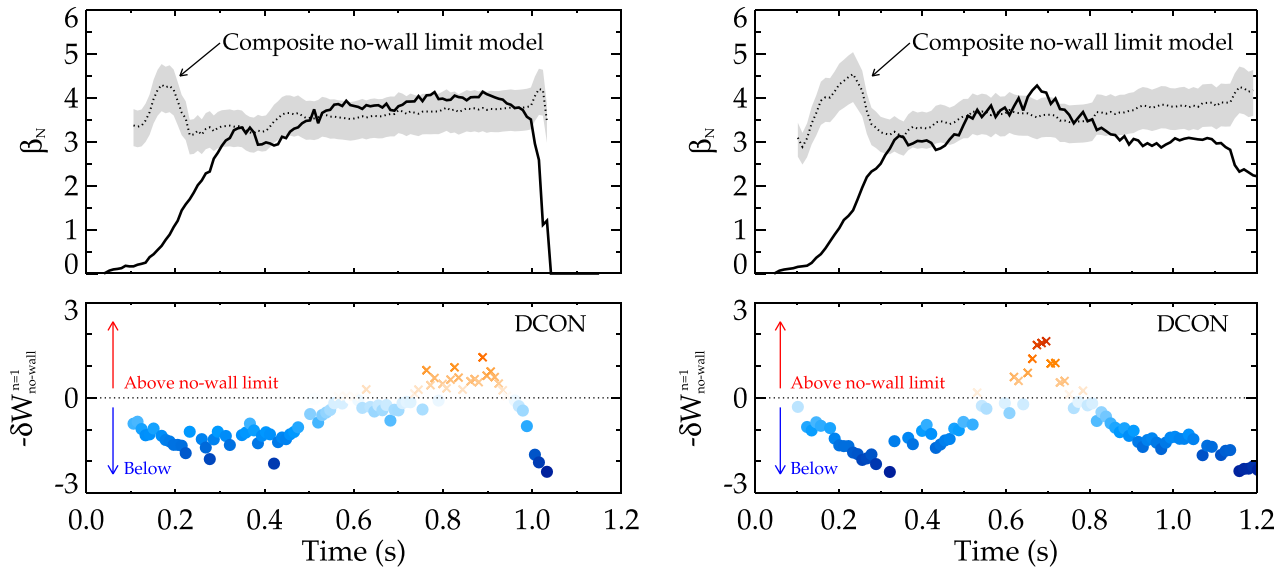

FIG. 2. Measured β_N and DECAF modelled $\beta_{N,\text{no-wall}}^{n=1}$ (dashed), and DCON calculated $-\delta W_{\text{no-wall}}^{n=1}$ vs. time for NSTX-U discharges 204112 (left) and 204118 (right). In the bottom panels the blue circles and red x'es indicate individual equilibria below and above the no-wall limit, respectively, with lighter colors indicating closer proximity to the limit.

results and the present, somewhat higher A NSTX-U plasmas.

The ideal model has been implemented in DECAF, and it replicates the analytical $\beta_{\mathrm{N,no-wall}}^{\mathrm{n=1}}$ limit in Ref. 16. Figure 3(a) shows the measured β_N for NSTX discharge 139514 along with the modelled no-wall and with-wall limits. It should be noted that presently all the model analysis described here is performed on post-processed equilibria, but it can easily accept equivalent real-time signals as well.

Knowledge of $\beta_{\mathrm{N,no-wall}}^{\mathrm{n=1}}$ provides the point at which $\delta W_{\mathrm{no-wall}}^{\mathrm{n=1}}$ crosses zero (from positive (stable) to negative (unstable)) as β_N increases. Here $\beta_N \equiv 10^8 \langle \beta_t \rangle a B_0 / I_p$, where $\beta_t \equiv 2\mu_0 \langle p \rangle / B_0^2$ is the toroidal beta, p is the plasma pressure, B_0 is the vacuum toroidal magnetic field at the plasma geometric center, and a is the plasma minor radius at the midplane. However, in order to estimate the RWM growth rate from Eq. (1), we require a model for $\delta W_{\mathrm{no-wall}}^{\mathrm{n=1}}$ as a function of plasma parameters. A heuristic expression of Hu and Betti[4] for the no-wall limit used $\delta W_{\mathrm{no-wall}}^{\mathrm{n=1}} \sim \beta_{\mathrm{N,no-wall}}^{\mathrm{n=1}} - \beta_N$. Alternatively in Ref. 16, many hundreds of experimental equilibria were run through DCON and a fit was made to $\delta W_{\mathrm{no-wall}}^{\mathrm{n=1}}$ vs. β_N and other parameters.[16] For example, when only pressure peaking was considered, at low values of $p_0/\langle p \rangle < 2.25$, $\delta W_{\mathrm{no-wall}}^{\mathrm{n=1}} = 2(1 - (\beta_N/(1.91 p_0/\langle p \rangle)))^3)$ was found ($\langle\rangle$ represents volume average). This analysis revealed a difference between the DCON $\delta W_{\mathrm{no-wall}}^{\mathrm{n=1}}$ and the heuristic expression in that the DCON results tended to saturate for low beta below the no-wall limit at stable, positive values of $\delta W_{\mathrm{no-wall}}^{\mathrm{n=1}}$. In other words, there is a ceiling on the stability level of any given plasma and it is difficult to continue to make a plasma even more stable, which intuitively makes sense.

One possible issue with using the DCON-based equation for δW as a function of β_N is that at high beta approaching the with-wall limit it does *not* saturate, but rather continues to grow quite large.[20] This implies (Eq. (1)) a very large fluid growth rate, which would make it very difficult for kinetic effects to stabilize the plasma at high beta, in contrast to experimental observations. Therefore we conclude that DCON calculations of $\delta W_{\mathrm{no-wall}}^{\mathrm{n=1}}$, which until now were almost exclusively used for determining the zero-crossing (no-wall limit), are very reasonable below or near the no-wall limit, but possibly not accurate well above it. In order to allow experimentally observed kinetic stabilization we propose to use in our present reduced model a simple expression for $\delta W_{\mathrm{no-wall}}^{\mathrm{n=1}}$ as a function of β_N

$$\delta W_{\mathrm{no-wall}}^{\mathrm{n=1}} = 2\tanh\left(\frac{\pi}{2}(-C_\beta)\right), \tag{2}$$

where C_β is the familiar parameter $(\beta_N - \beta_{\mathrm{N,no-wall}}^{\mathrm{n=1}})/(\beta_{\mathrm{N,with-wall}}^{\mathrm{n=1}} - \beta_{\mathrm{N,no-wall}}^{\mathrm{n=1}})$. We will see that this expression captures the essential dependencies of DCON while also permitting interesting and complex stability behavior when kinetic effects are included.

The quantity C_β is shown in Fig. 3(b) for NSTX discharge 139514, and $\delta W_{\mathrm{no-wall}}^{\mathrm{n=1}}$ is shown in Fig. 3(c). Also shown in Fig. 3(b) is a moving average of C_β. The moving average, which we will also employ on other quantities later, provides a considerably smoother signal, with the tradeoff of a time lag because the average is causal (using only previous time points) for compatibility with future real-time systems. Here the average was taken over 10 time points of 8 ms resolution.

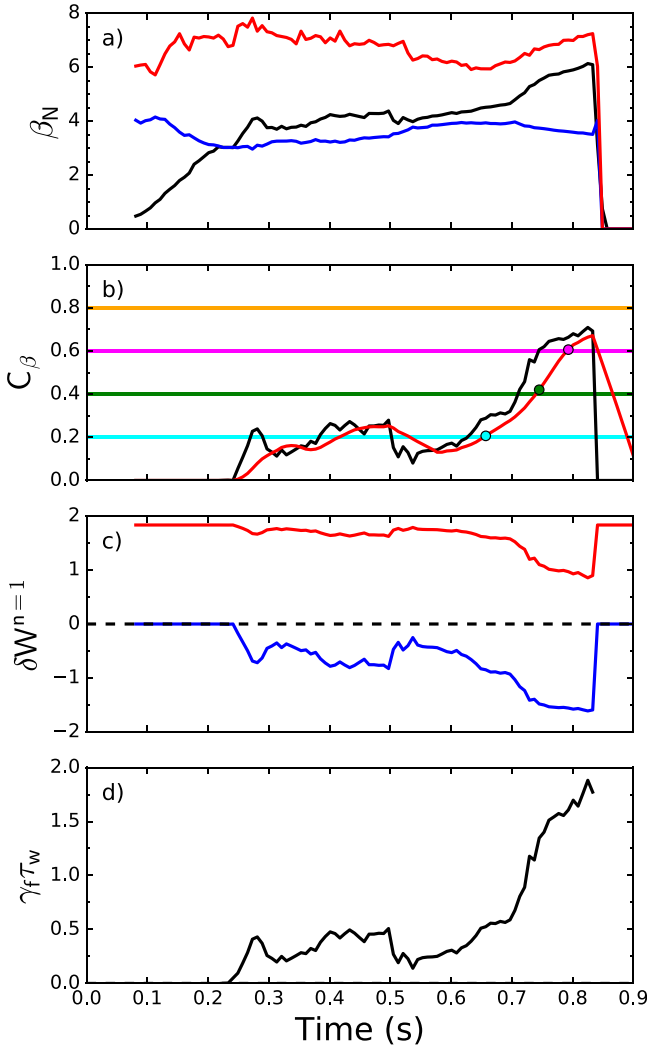

FIG. 3. (a) Measured β_N (black) and DECAF modelled $\beta_{\mathrm{N,with-wall}}^{\mathrm{n=1}}$ (red) and $\beta_{\mathrm{N,no-wall}}^{\mathrm{n=1}}$ (blue); (b) C_β calculated from the quantities in frame a (black) along with a moving average (red) and colored markers indicating where C_β crosses certain levels; (c) $\delta W_{\mathrm{with-wall}}^{\mathrm{n=1}}$ (red) and $\delta W_{\mathrm{no-wall}}^{\mathrm{n=1}}$ (blue); and (d) normalized ideal fluid growth rate vs. time for NSTX discharge 139514.

IV. IDEAL WITH-WALL LIMIT

Having determined, in Sec. III, a model for $\delta W_{\mathrm{no-wall}}^{\mathrm{n=1}}$ that can be used for δW_∞ in Eq. (1), we now turn to $\delta W_{\mathrm{with-wall}}^{\mathrm{n=1}}$ for δW_b, starting again by examining the beta limit. An expression for the fluid with-wall β limit was not examined in Ref. 16, but a simple model can be provided here. Previously, the with-wall β limit has been computed for NSTX in four different high performance discharge scenarios by scaling pressure profiles and running DCON with the wall.[21] In that case it was noted that the with-wall β limit tracked the continuous evolution of the current profile, such that as internal inductance (a measure of the peakedness of the current profile) increased with time during the

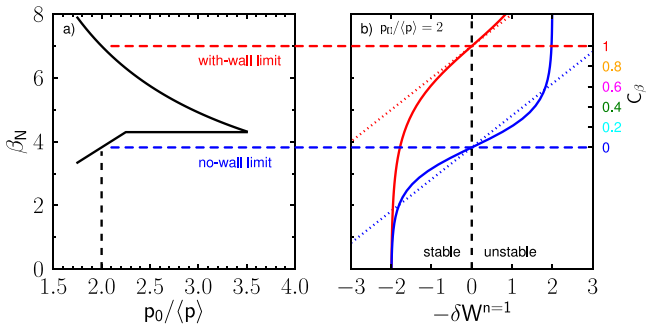

FIG. 4. (a) No-wall and with-wall β_N limits for NSTX vs. pressure peaking only, given by $\beta_{N,no-wall}^{n=1} = 1.91 p_0/\langle p\rangle$ $(p_0/\langle p\rangle < 2.25)$ and $\beta_{N,no-wall}^{n=1} = 4.3$ $(p_0/\langle p\rangle > 2.25)$,[16] and $\beta_{N,with-wall}^{n=1} = 0.75 + 12.5/p_0/\langle p\rangle$. (b) β_N vs. $-\delta W^{n=1}$ for NSTX at $p_0/\langle p\rangle = 2$, showing the heuristic expression of Ref. 4 in dotted lines and present reduced model in solid lines, with red for $\delta W_{with-wall}^{n=1}$ and blue for $\delta W_{no-wall}^{n=1}$.

discharges, $\beta_{N,with-wall}^{n=1}$ decreased. Subsequently, in projected with-wall β limit calculations for NSTX-U it was noted that the with-wall β limit decreased with increasing pressure peaking as well.[22] These two trends are related, as there is an experimental correspondence between pressure and current peaking.[16] This behavior of the with-wall β limit is in contrast to the trends of the no-wall β limit with pressure peaking and internal inductance, which tend to increase at low peakedness before flattening off.[16] Therefore, the expected gap between the no-wall and with-wall $n = 1$ β limits is considerably wider with broad current and pressure profiles, and narrower with more peaked profiles.[23,24] This behavior can be seen in Fig. 4(a), which shows the previously derived $\beta_{N,no-wall}^{n=1}$ limit with pressure peaking dependence only[16] and the $\beta_{N,with-wall}^{n=1}$ limit that will be presently described.

The with-wall limit is also evident in an operational limit on β with increasing pressure peaking which can be seen clearly in Fig. 3 of Ref. 16 (these effects should also be seen in ITER[25]). In fact, the fit to the DCON calculated projected with-wall limit for NSTX-U found in Ref. 22, $\beta_{N,with-wall}^{n=1} = 0.2 + 12.5/(p_0/\langle p\rangle)$, also approximates the operational limit seen in NSTX. Therefore, for the present purpose we will use a similar estimate for $\beta_{N,with-wall}^{n=1}$, without adding a dependence on internal inductance since this will not add much to the estimate because of the aforementioned correspondence between the two parameters.

Similar to the no-wall δW analysis, an analysis of hundreds of experimental equilibria from NSTX has now been performed with DCON including a conducting wall. A similar stable, positive saturation of the with-wall limit was also found. Also, it was seen that the plasmas stayed below the with-wall limit to a slightly higher level of β_N than the estimate for NSTX-U from Ref. 22, which makes sense considering the lower aspect ratio of NSTX.[16] Therefore, the model we will use for the with-wall β limit is $\beta_{N,with-wall}^{n=1} = 0.75 + 12.5/(p_0/\langle p\rangle)$. In addition to the previously derived no-wall β limit estimate, Fig. 3(a) shows the with-wall β, which has also been recently implemented in DECAF.

For $\delta W_{with-wall}^{n=1}$ a similar dependence to that for the no-wall δW will be used, here with $1 - C_\beta$ for the with-wall limit

$$\delta W_{with-wall}^{n=1} = 2\tanh\left(\frac{\pi}{2}(1 - C_\beta)\right). \quad (3)$$

This with-wall δW is also shown in Fig. 3(c) for NSTX discharge 139514. The no-wall (blue) and with-wall (red) δW terms calculated in this way are compared with the linear heuristic model for the NSTX case at $p_0/\langle p\rangle = 2$ in Fig. 4(b). Negative δW is plotted here to more intuitively show the change from stable to unstable as β_N is increased. Note that both δW curves saturate at low β, as is seen in DCON calculations, and both are quite close to the heuristic model near the zero crossings. The new feature is that $\delta W_{no-wall}^{n=1}$ saturates near the with-wall limit as opposed to continuing to greatly increase.

Finally, the fluid growth rate of the RWM, $\gamma_f \tau_w$ (from Eq. (1) with $\delta W_K = 0$), is shown in Fig. 3(d). Of course, as has been demonstrated, the fluid growth rate of the RWM cannot explain its stability; modifications to ideal stability by kinetic effects are necessary.[16]

V. GENERAL BEHAVIOR OF THE RWM GROWTH RATE MODEL

Now that expressions for δW_∞ and δW_b have been determined, once the kinetic term δW_K is defined, the kinetic growth rate, $\gamma \tau_w$ can be calculated from Eq. (1). Without yet defining δW_K we can also, however, now demonstrate the consequences of the present reduced model fluid terms on stability. Figure 5(a) shows a stability diagram in $Im(\delta W_K)$ vs. $Re(\delta W_K)$ space in which the unstable regions (inside the circles) are defined by the fluid terms[9] (the radius of the circles $r = \frac{1}{2}(\delta W_b - \delta W_\infty)$, while the offset $a = \frac{1}{2}(\delta W_b + \delta W_\infty)$. In other words, the diameter of the circle is given by the horizontal gap between the red and blue δW curves in Fig. 4(b), at a given C_β, while the origin of the circle is given by the midpoint between those curves. One can see in Fig. 5(a) that the unstable region shifts from negative $Re(\delta W_K)$ space to positive as C_β is increased from the no-wall to the with-wall limits, while the size of the region increases and then decreases again.

Finally, using sample levels of δW_K, we can see the predicted RWM kinetic growth rate of this model, shown in Fig. 5(b). With $Re(\delta W_K) = Im(\delta W_K) = 0$, the fluid growth rate is recovered, which increases asymptotically as C_β goes from 0 to 1. However, when finite kinetic effects are introduced the behavior changes. With a sufficiently large level of kinetic effects, shown by the "X" marker in Fig. 5(a), the plasma is robustly stable. With $Re(\delta W_K) = Im(\delta W_K) = 0.5$ (square marker), it takes $C_\beta = 0.2$ for the unstable region to overtake the kinetic stability. With $Re(\delta W_K) = Im(\delta W_K) = 1.0$ (triangle marker), it takes $C_\beta = 0.6$ for instability and then at higher $C_\beta \approx 0.9$ the unstable region shrinks and the plasma is stable again. This behavior means that for a given level of kinetic stability, it is possible for a plasma to be more stable at lower beta and higher beta, but less stable in between (a behavior observed in some experiments[2]). This—it should be reemphasized—is with a constant level of kinetic stability; i.e., no evolution to a favorable rotation profile (for example) must be invoked to explain this behavior. Of course as a plasma evolves in time its kinetic effects *will*

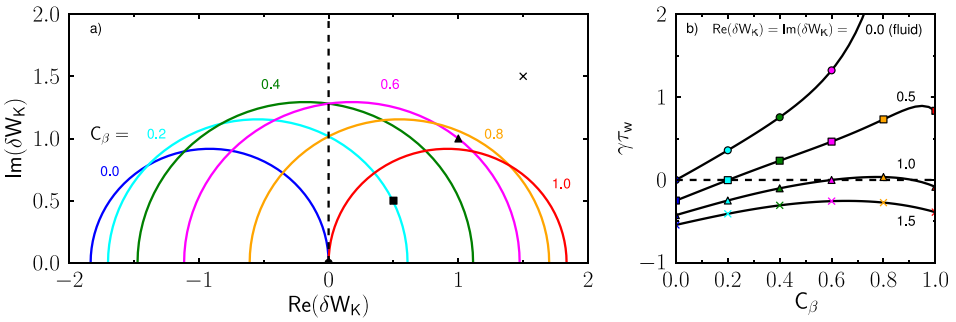

FIG. 5. (a) Kinetic RWM stability diagram for NSTX at $p_0/\langle p\rangle = 2$. The circles represent the unstable region for various values of C_β. (b) Normalized growth rate vs. C_β for four levels of kinetic effects, indicated by markers in (a).

change and so the experimental "marker" of the plasma will move in the kinetic space of the stability diagram or Fig. 5(a), even as the size and location of the unstable region is also changing in time. We turn now to a discussion of the strategy for completing the reduced model for forecasting RWM stability in real time by estimating δW_K.

VI. THE REDUCED KINETIC MODEL

For the kinetic δW_K term, full calculations with codes such as MISK cannot be performed in real time, as these calculations can take tens of minutes to complete. Kinetic RWM stability theory has continued to be developed, yielding greater complexity in recent years by the inclusion of additional terms from such effects as anisotropy of the plasma pressure[26] and additional fluid[27] and kinetic[28] rotational effects. Here we wish to go in the *opposite* direction and simplify kinetic theory to facilitate real-time calculation while still retaining a high level of accuracy suitable to serve a physics-based, improved disruption avoidance system for the tokamak. The time scale requirements for a real-time system are based on multiple considerations, the mode growth rate, control system reaction time, control coil time scales, and the momentum diffusion time for rotation control, for example, and these range from tens of milliseconds in NSTX to longer time scales in larger devices such as ITER (in the range of seconds).

It was previously recognized that simplified model calculations based on physics insight from kinetic stability theory should be examined.[2,16] As one example, a very simple forecast for RWM stability might involve monitoring only the $E\times B$ frequency in real-time and comparing with ranges of stabilizing bounce or precession frequency resonances.

A more sophisticated model with collisionality,[17] plus the addition of the effect of energetic particles[10] on the real part of δW_K, will now be described. The reduced kinetic model results, in terms of timing of warnings for impending RWM instability, will then be tested against an independently characterized NSTX database of RWM disruptions. Ultimately the model's effectiveness will be judged by its ability to accurately forecast RWM stability while still being lean enough to easily run in real-time for multiple devices.

A previous effort to simplify the dispersion relation to examine the nature of the roots of the equation[29] made the following simplifications. First, separation of the energetic and thermal particle contributions is natural, due to the very different kinetic frequencies with respect to the plasma rotation. Second, experience shows that at the relatively low rotation levels in most present (and nearly all future) devices, the most important type of kinetic resonance for RWM stability is that between the plasma rotation and trapped particles with no bounce harmonic ($l=0$), but a precession drift motion. Further, although profile effects certainly matter (kinetic theory has shown that the rotation *profile* is important rather than a scalar "critical" rotation[9]), for simplicity in the present model we have chosen to omit the radial dependence of the variables. We will show that, based upon experimental experience with NSTX,[2] using average values inside the density pedestal is a reasonable way to accomplish this. In the following $\langle\omega_E\rangle$ and $\langle\nu\rangle$ represent these average values for $E\times B$ frequency and collisionality as described in Ref. 2. Additionally, full experimental radial profiles of necessary measured quantities such as rotation may not be available (for example, the real-time velocity diagnostic for NSTX[30,31] has four radial channels), so future real-time systems based on this reduced kinetic model should be able to operate with limited profile data. Finally, it is similarly necessary to neglect pitch angle dependencies of frequencies as well. This set of conditions leaves an expression for δW_K of trapped ions

$$\delta W_K \sim \int_0^\infty \left[\frac{\omega_{*N}+\left(\hat{\varepsilon}-\frac{3}{2}\right)\omega_{*T}+\omega_E-\omega_r-i\gamma}{\overline{\omega_D}\hat{\varepsilon}+l\overline{\omega_b}\hat{\varepsilon}^{\frac{1}{2}}-i\bar{\nu}\hat{\varepsilon}^{-\frac{3}{2}}+\omega_E-\omega_r-i\gamma}\right]\hat{\varepsilon}^{\frac{5}{2}}e^{-\hat{\varepsilon}}d\hat{\varepsilon}. \tag{4}$$

Here we have made the energy dependencies of the various terms explicit by utilizing $\bar{x}$, the constant value of x at $\hat{\varepsilon}=1$. Energy is normalized by temperature with $\hat{\varepsilon}=\varepsilon/T$, and ω_{*N} and ω_{*T} are, respectively, the density and temperature gradient components of the ion diamagnetic frequency.

Liu *et al.* have provided analytical solutions to the above expression for various cases. Some of the simplest of these are obtained in the limit of high plasma rotation[32] (also described in Ref. 33), by retaining both ions and electrons but neglecting collisions and energy dependence[34] (also described in Ref. 29), or by neglecting collisionality and plasma rotation[32] (note that this situation is most justified for energetic particles and results in a δW_K independent of ω_E and ν, similar to what we will ultimately use).

In the present model we wish to make simplifying assumptions, but we must retain the most critical physics elements based on experience applying the full theory to tokamak experiments. Therefore while neglecting the growth

rate and real mode frequency (γ and ω_r) as much smaller than ω_E and neglecting the electron contribution as much smaller than the ion one (electron collisionality is $\sqrt{m_i/m_e}$ higher) are justified, neglecting collisions outright is not. In fact attempts have already been made to examine collisionality in simplified models, and there it was shown that collisions can play an unexpected role—damping the stabilizing kinetic effects.[17] That work also demonstrated that although energy-dependent collisionality is the most complete model, energy-independent collisionality can give similar results.[17] Using energy-independent collisionality, Eq. (4) can also be solved analytically, as was first demonstrated by Liu *et al.*,[32] and results in various expressions for the integral in Eq. (4) for regimes such as $l=0$ trapped particles with precession motion only, $l\neq 0$ trapped particles with $\omega_D \ll \omega_b$, and circulating particles with $\omega_D \ll \omega_t$ (the transit frequency). These result in complex analytical solutions relying on calculations of the plasma dispersion function[32] (in fact these functions were compared and benchmarked between the MISK, MARS–K, and PENT codes in Sec. V and Fig. 10 of Ref. 33).

Further simplification of the equation for δW_K by neglecting energy dependence in the precession and bounce frequencies has also been performed and used to gain insight on the role of collisions near and away from stabilizing resonances (see Eqs. (5) and (6) of Ref. 17). However, such a simplification loses some of the behaviours of the full model (for example, the resonant term in Eq. (6) of Ref. 17). Though useful for gaining physics insight, at this point it becomes clear that strictly simplifying equations to reach the possibility of analytical solution does not serve the present purpose. Instead it is much more meaningful to construct, from scratch, a functional form that is easily, quickly calculable and that relies on a few important, measurable parameters. Any such model must capture the essential physics learned from the successful application of kinetic theory to experimental results in recent years, namely:

- Resonance between ω_E and ω_D of trapped thermal ions at lower plasma rotation and with ω_b at higher plasma rotation provides a stabilizing component to δW_K, but in between these the kinetic effects are weaker, allowing for instability.[2,9]
- Energetic particles provide a stabilizing restorative force that is relatively independent of plasma rotation[10] and the collisionality of those particles.[17]
- Increased collisionality tends to damp the rotational resonance stabilization (see Fig. 3 of Ref. 17) and shift it to slightly lower rotation (see Fig. 6 of Ref. 9).
- The imaginary term of δW_K from trapped thermal ions tends to peak at lower plasma rotation than the real part (see Fig. 8 of Ref. 10) so that plasmas move in kinetic stability space as rotation changes in looping paths (see Fig. 5 of Ref. 9).

To that end, Gaussian functions were used to represent kinetic resonances in the present model. In the present work resonances between the plasma rotation and thermal particle motions are represented; energetic particles are not yet included. The positions of the peaks in $\langle\omega_E\rangle$ are determined by typical experimental ranges of ω_D and ω_b, and the height, width, and position all dependent on collisionality. The bounce resonance contribution was allowed to continue to increase at high $\langle\omega_E\rangle$ to capture the many bounce harmonics and circulating particle contributions which provide stability at large rotation.

TABLE I. Gaussian coefficients for Eq. (4) for the reduced kinetic model for NSTX.

	a	b	c
$Re(\delta W_K)$ precession	6	$\dfrac{1}{1+\left(\frac{4}{9}\frac{\langle\nu\rangle}{\omega_D}\right)^2}$	$\frac{3}{5}\left(1+\frac{2}{9}\frac{\langle\nu\rangle}{\omega_D}\right)$
$Im(\delta W_K)$ precession	4.5	$\frac{3}{4}\left[\dfrac{1}{1+\left(\frac{4}{9}\frac{\langle\nu\rangle}{\omega_D}\right)^2}\right]$	$\frac{3}{5}\left(1+\frac{2}{9}\frac{\langle\nu\rangle}{\omega_D}\right)$
$Re(\delta W_K)$ bounce	$\dfrac{1+25\frac{\langle\nu\rangle}{\omega_b}}{1+\left(\frac{25}{8}\frac{\langle\nu\rangle}{\omega_b}\right)^2}$	$\dfrac{11}{6+75\frac{\langle\nu\rangle}{\omega_b}}$	$\frac{1}{5}+\frac{125}{128}\left(\frac{\langle\nu\rangle}{\omega_b}\right)^2$
$Im\ (\delta W_K)$ bounce	$\frac{4}{7}\left[\dfrac{1+25\frac{\langle\nu\rangle}{\omega_b}}{1+\left(\frac{25}{8}\frac{\langle\nu\rangle}{\omega_b}\right)^2}\right]$	$\frac{7}{8}\left[\dfrac{11}{6+75\frac{\langle\nu\rangle}{\omega_b}}\right]$	$\frac{1}{5}+\frac{125}{128}\left(\frac{\langle\nu\rangle}{\omega_b}\right)^2$

The functional forms for the real and imaginary, precession and bounce δW_K terms are

$$\delta W_K = a\frac{\langle\omega_E\rangle}{\omega}e^{\frac{-\left(\frac{\langle\omega_E\rangle}{\omega}-b\right)^2}{2c^2}}, \tag{5}$$

where the normalizing ω is a representative value of ω_D or ω_b, respectively. For the NSTX analysis, these quantities were taken to be $\omega_D = 2$ kHz and $\omega_b = 10$ kHz. The quantities a, b, and c, pertaining, respectively, to the height, position, and width of the peaks are given for this instance of the model for NSTX in Table I. Coefficients for the functions were selected to reflect experience with MISK calculations for NSTX, and their forms were chosen to give the typical dependencies on particle frequencies. Additionally, at large

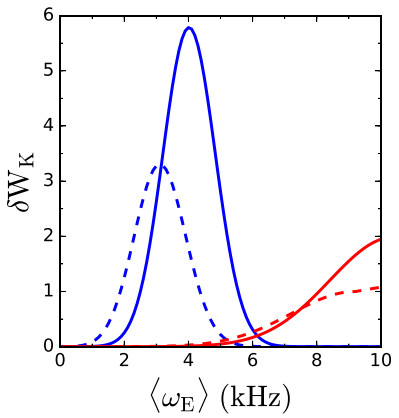

FIG. 6. Real (solid) and imaginary (dashed) parts of modelled δW_K for precession resonance (blue) and bounce resonances (red) for NSTX with $\langle\nu\rangle = 1$ kHz.

rotation (greater than the bounce peak) the bounce δW_K term simply increases like $0.1(\langle\omega_E\rangle - \langle\omega_E\rangle_{peak})$. Figure 6 shows an example of these Gaussians for an NSTX case at $\langle\nu\rangle = 1$ kHz.

Now that the form of δW_K versus these quantities is established in the model, it is left to implement the model by following the evolution of a plasma discharge in time through the space of these quantities. Additionally, for the fluids terms the previously discussed quantities of $p_0/\langle p\rangle$, l_i, A, and β_N must also be followed. The procedure is simply laid out as such:

(1) Quantities l_i, $p_0/\langle p\rangle$, and A are used in the ideal beta limit model to calculate $\beta_{N,no-wall}$ and $\beta_{N,with-wall}$ (Fig. 3(a)).
(2) These ideal β limits and the measured β_N give C_β (Fig. 3(b)).
(3) Expressions for the fluid δW terms as functions of C_β that mimic DCON results give δW_b and δW_∞ (Eqs. (2) and (3) and Fig. 3(c)).
(4) The ideal δW terms give the fluid growth rate, $\gamma_f\tau_w$ (Fig. 3(d)), and also set the unstable region in a $Im(\delta W_K)$ vs. $Re(\delta W_K)$ stability diagram (Fig. 5(a)).
(5) Calculated $\langle\omega_E\rangle$ and $\langle\nu\rangle$ are used in the reduced kinetic model (Eq. (4)) to calculate δW_K.
(6) Finally, δW_K is used in the kinetic RWM dispersion relation (Eq. (1)) to find $\gamma\tau_w$.

Therefore, for step 5 we now show $\langle\omega_E\rangle$ and $\langle\nu\rangle$ vs. time for NSTX discharge 139514 in Fig. 7. Note that the quantities shown in the plots are moving averages (as described for C_β in Fig. 3(b)) for clarity of presentation, but the quantities used as inputs to the calculation of δW_K (and subsequently $\gamma\tau_w$) are used at the available higher resolution time points and not the moving average values.

Through the changing levels of total (precession plus bounce terms) real and imaginary δW_K, as in Fig. 6, one can then plot the trajectory of the plasma in $Re(\delta W_K)$ vs. $Im(\delta W_K)$ space. This is shown in Fig. 8 along with the unstable regions for various levels of C_β. The circular lines indicating the unstable boundary correspond to $\gamma\tau_w = 0$. Inside these circles $\gamma\tau_w$ is positive, and therefore the kinetic RWM

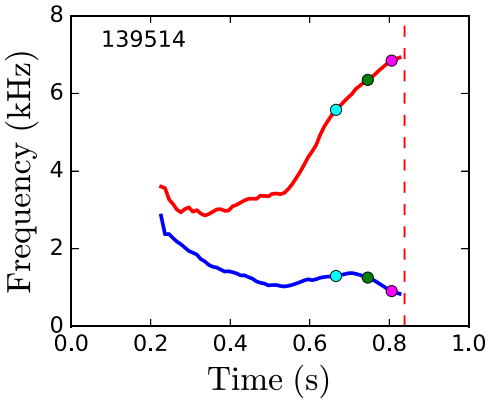

FIG. 7. Moving averages of $\langle\omega_E\rangle$ (red) and $\langle\nu\rangle$ (blue) for NSTX discharge 139514 vs. time. The colored markers indicate the point at which the plasma reaches the correspondingly colored C_β levels as in Fig. 3(b).

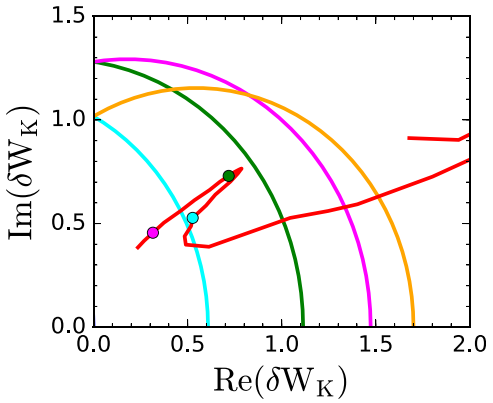

FIG. 8. Time-varying stability diagram for NSTX discharge 139514 where the colored circles indicate the unstable region at different levels of C_β (using the colors in Fig. 3(b)). The red line indicates the moving average of the trajectory of the plasma through complex δW_K space with time and the colored markers indicate the point at which the plasma reaches the correspondingly colored C_β levels.

is unstable. It must be remembered that as the plasma parameters change in time in the δW_K space, at the same time the size of the unstable region is changing as well. Within the plasma trajectory shown, colored circular markers are placed indicating the times that the plasma crosses the corresponding C_β level (Fig. 3(b)). So, for example, in this case at the time in the discharge when $C_\beta = 0.2$ (cyan) the plasma is just outside the unstable region while by the times of $C_\beta = 0.4$ (green) and $C_\beta = 0.6$ (magenta), δW_K has decreased due to the changing $\langle\omega_E\rangle$ and $\langle\nu\rangle$ and additionally the unstable region has increased in size due to the fluid terms at the larger C_β. The combined effect is that the plasma is now inside the unstable region.

Alternatively, one can show a stability diagram in the $\langle\omega_E\rangle$ vs. $\langle\nu\rangle$ space at a given level of C_β by plotting contours of $\gamma\tau_w$ (similar to Fig. 6 in Ref. 9). These contours are calculated for the entire space because the location in $(\langle\omega_E\rangle, \langle\nu\rangle)$ determines δW_K in the reduced kinetic model and for a given C_β this determines $\gamma\tau_w$. Here we show the trajectory of the same plasma in this space as time increases and $\langle\omega_E\rangle$ increases while $\langle\nu\rangle$ decreases (Fig. 9). Similarly to Fig. 8, in this type of diagram the unstable region changes with time as C_β changes. Here we use the same colored lines to indicate the expanding unstable region, and one can see the same crossing of the plasma into the unstable region as in Fig. 8.

VII. APPLICATION OF THE MODEL TO AN NSTX DATABSE

It is worth restating that all of the above analysis and plotting has been performed post-discharge on NSTX data. The coding of the analysis is written in such a way that it could be implemented in exactly the same manner in a future real-time system with the appropriate real-time diagnostics for input. The future goal is to implement this model in real time, in which case the crossing (or even the approach) to the unstable region would be used in a disruption avoidance system to trigger a plasma control system (for example,

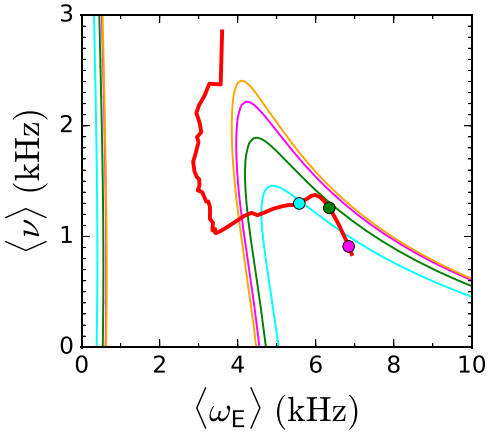

FIG. 9. Trajectory of NSTX discharge 139514 through $\langle\omega_E\rangle$ vs. $\langle\nu\rangle$ space, with colored regions and markers as in Fig. 8.

plasma rotation control) to maintain stability. Disruption avoidance via plasma rotation profile control[12] is close to becoming reality in NSTX-U with the recent implementation of real-time velocity diagnostics.[30,31]

In the meantime, however, it is useful to apply the reduced model to a database of NSTX RWM discharges to determine how accurately the marginal stability point of the kinetic RWM is evaluated. For a large number of discharges we will presently show their trajectories on a stability map as in Fig. 9. Also it is natural to simply plot the RWM growth rate forecast from these trajectories as a function of time (the kinetic equivalent of the ideal growth rate shown in Fig. 3(d)). Here, for unstable discharges, we plot $\gamma\tau_w$ vs. time before the DIS event warning (the time of disruption, as determined by tests within DECAF). For discharges without an RWM induced disruption, we simply plot $\gamma\tau_w$ vs. time.

These plots are shown in Fig. 10 for 20 discharges with unstable RWMs in NSTX and in Fig. 11 for 8 without. Unstable RWMs were determined to have occurred in these discharges by both independent assessment of relevant signals as well as a threshold test on a poloidal magnetic signal within DECAF (DECAF characterization of disruption event chains, including the RWM event, will be the subject of a separate paper). The colors indicate the warning time before

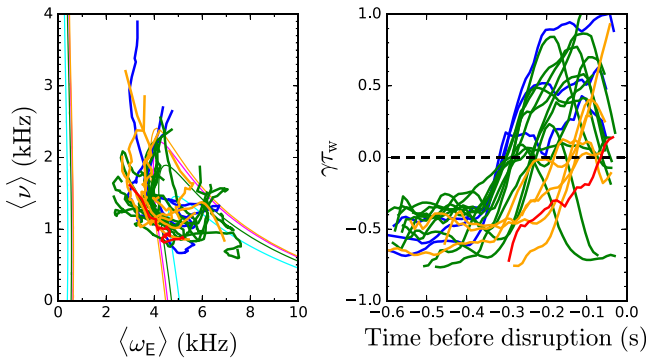

FIG. 10. Stability diagram (left) and forecast growth rate vs. time leading to disruption (right) for unstable NSTX discharges that were predicted unstable within 0.32 s of the disruption time by the reduced kinetic model.

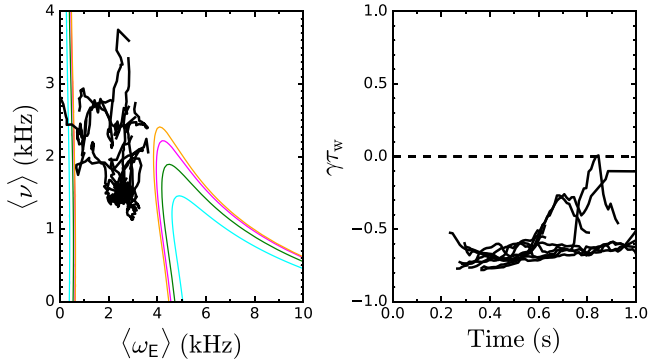

FIG. 11. Stability diagram (left) and forecast growth rate vs. time (right) for stable NSTX discharges that were predicted stable by the reduced kinetic model.

disruption when the model indicates the RWM should be unstable ($\gamma\tau_w$ crosses zero). Red is for a single case of <0.1 s warning, orange five cases with 0.1–0.2 s, green eleven cases with 0.2–0.3 s, and blue three cases with 0.3–0.32 s warning. These time scales are all sufficient to take action to avoid a disruption. For example, the alteration of the rotation profile toward stable plasma regimes has been shown to be theoretically possible with rotation control feedback planned for NSTX-U as quickly as one half of the momentum diffusion time—on the order of 0.02 s.[12] Additionally, the RWM control system on NSTX routinely demonstrated mode control on mode growth rate timescales as quickly as a few milliseconds.[13]

One can see quite clearly a difference in the evolution in $\langle\nu\rangle$, $\langle\omega_E\rangle$ space between the stable and unstable discharges. While all the discharges drop in collisionality with time as they evolve, due to increasing temperature, in the unstable cases a turn towards higher $\langle\omega_E\rangle$ leads into the unstable region. This is avoided in all the stable cases shown here (in fact, some drop towards zero $\langle\omega_E\rangle$ leading one case to just barely touch $\gamma\tau_w = 0$).

In addition to the cases shown in Fig. 10, many others were analyzed. In fifteen additional RWM unstable cases, the model also showed $\gamma\tau_w$ crossing zero into the unstable region, but in these cases this occurred well before the disruption and in fact were all correlated with *minor* disruptions that occurred earlier in those shots. Here a minor disruption is defined as a 10% drop in both β_N and stored energy within 0.1 s, that subsequently recovers. In each of the fifteen cases considered, $\gamma\tau_w$ crossed zero within 0.1 s of a minor disruption. There were, however, other minor disruptions in the total database of shots that did not correlate with the reduced kinetic model warning; whether these are due to other causes will be further explored.

In any case, there were 35 discharges in the database where the RWM became unstable leading to a disruption in which the reduced kinetic model predicted instability within 0.32 s of the disruption or 0.1 s of an earlier minor disruption. Additionally in three experimentally RWM unstable cases, the model gave a warning >0.4 s in advance without any related minor disruption, which we consider a false positive because it occurs highly separated (earlier) in time from the time of DIS. Finally, this initial model sometimes misses

unstable RWMs. There was one case in which $\gamma\tau_w$ barely did not cross zero, three cases with very low C_β disruptions that the model missed, and three cases where $\langle\omega_E\rangle$ was in what the model considered to be a stable range, yet an unstable RWM occurred. Altogether the model failed to predict an unstable RWM at all in 7 out of 45 experimentally unstable cases, or 15.6%. The success rate of the model is surprisingly high given its initial state and relative simplicity, and that it has not been optimized. Further research will aim to improve the success rate.

Finally, in addition to the eight successful predictions of stability for the experimentally *stable* discharges shown above, five more stable discharges were tested. In three of these cases the discharge evolution in $\langle\nu\rangle$, $\langle\omega_E\rangle$ space was very similar to the *unstable* cases shown in Fig. 10, but nevertheless the discharge remained stable. It is possible that in these cases some other stabilizing effect not captured by the reduced model was present, but this remains to be determined. In two other experimentally stable cases, the RWM warning was triggered by the reduced model because $\langle\omega_E\rangle$ went to zero (hints of this behavior also appear in some of the discharges in Fig. 11). The unstable region at $\langle\omega_E\rangle \sim 0$ is present in the model due to theory expectation, but has not yet usefully captured an unstable RWM in our NSTX analysis. This region could be eliminated in the model since we are interested in improving the model's usefulness whether or not it agrees perfectly with theory, but this requires further investigation. If those cases were eliminated then 10 out of 13, or 77%, of stable high β, long-pulse NSTX discharges analyzed were predicted stable in the reduced model.

In addition to the application of the reduced model for real time warning of plasma stability, another future goal is to use this model for a larger database analysis. In addition to the cases described above, the fast application of the model will allow analysis of very large databases from all of NSTX operation, or operation of other devices, which may reveal insight that is difficult to obtain from more complicated and slower calculations of a smaller number of cases.

VIII. DISCUSSION AND CONCLUSIONS

A reduced kinetic RWM model has been derived that does well in initial tests to reproduce experimental kinetic RWM marginal stability points in NSTX. There are several elements of the present reduced kinetic model that may be improved. First, some factors are presently missing that may be added in the future to improve the accuracy, such as the effect of energetic particles. Second, the need for relative simplicity may naturally mean that the dynamics of instability in some cases is missed. For example, in the present model the parameters ω_D and ω_b are left constant for all plasmas in a given machine (here NSTX). In some cases, then, the unstable region in the stability diagram must be not quite correct. One might imagine in the future these parameters could change from shot to shot, and in time as well, but this would add a large degree of complexity to the model. We have taken the approach that what is most important is having a broad model which can encompass most of the common RWM instability issues. False positives or early warnings may mean that an actuator based on this model will sometimes unnecessarily act upon the plasma when it was still stable (changing the rotation profile back to a "safer" profile, for example), but this is perfectly acceptable because the actuation is not meant to be a disruptive mitigation, such as massive gas injection. In the present model we have purposefully made a larger unstable region to minimize missed instabilities. This does lead to an abundance of early warnings. For example, here we have considered warnings up to 0.32 s prior to disruption to be legitimate RWM warnings, despite that this is a long time scale compared with the dynamics of the mode. Again, this is considered acceptable because of the conservative nature of the response to the warnings. Despite the large unstable region, the simplicity of the model may mean that it sometimes misses RWM instabilities (as we have seen in the database). This may also be acceptable, though, if the reduced model is not the only piece of the disruption avoidance system focused on RWMs. For example, active feedback and a physics-based state-space controller[3] should also be operating at the same time.

In conclusion, a reduced kinetic stability model has been implemented in DECAF with the ultimate goal of real-time RWM stability forecasting. The model is based upon the successful kinetic modification of ideal stability theory and replicates, more simply, the effects of stabilizing resonances of mode-particle interaction in $E \times B$ frequency, collisionality space. The reduced model also incorporates parameterized models for the ideal no-wall and with-wall stability limits, which are shown to be in good agreement with DCON code calculations. The model has been tested on a database of NSTX discharges including discharges experimentally stable and unstable to the RWM. Good success has been achieved to date in separating those discharges on the stability map, predicting unstable discharges as unstable in the model and stable discharges as stable.

ACKNOWLEDGMENTS

The authors would like to acknowledge the diagnostic contributions of A. Diallo and M. Podesta. This research was supported by the U.S. Department of Energy under Contract Nos. DE-FG02-99ER54524 (Columbia University) and DE-AC02-09CH11466 (Princeton Plasma Physics Laboratory). The digital data for this paper can be found at http://arks.princeton.edu/ark:/88435/dsp01dj52w7187.

[1]H. Reimerdes, M. S. Chu, A. M. Garafalo, G. L. Jackson, R. J. La Haye, G. Navratil, M. Okabayashi, J. T. Scoville, and E. J. Strait, Phys. Rev. Lett. **93**, 135002 (2004).
[2]J. W. Berkery, S. A. Sabbagh, A. Balbaky, R. E. Bell, R. Betti, A. Diallo, S. P. Gerhardt, B. P. LeBlanc, J. Manickam, J. E. Menard, and M. Podesta, Phys. Plasmas **21**, 056112 (2014).
[3]S. A. Sabbagh and NSTX Team, Nucl. Fusion **53**, 104007 (2013).
[4]B. Hu and R. Betti, Phys. Rev. Lett. **93**, 105002 (2004).
[5]B. Hu, R. Betti, and J. Manickam, Phys. Plasmas **12**, 057301 (2005).
[6]Y. Liu, M. S. Chu, I. T. Chapman, and T. C. Hender, Phys. Plasmas **15**, 112503 (2008).
[7]I. T. Chapman, C. G. Gimblett, M. P. Gryaznevich, T. C. Hender, D. F. Howell, Y. Q. Liu, and S. D. Pinches, Plasma Phys. Controlled Fusion **51**, 055015 (2009).
[8]S. A. Sabbagh, J. W. Berkery, R. E. Bell, J. M. Bialek, S. P. Gerhardt, J. E. Menard, R. Betti, D. A. Gates, B. Hu, O. N. Katsuro-Hopkins, B. P.

LeBlanc, F. M. Levinton, J. Manickam, K. Tritz, and H. Yuh, Nucl. Fusion **50**, 025020 (2010).
[9]J. W. Berkery, S. A. Sabbagh, R. Betti, B. Hu, R. E. Bell, S. P. Gerhardt, J. Manickam, and K. Tritz, Phys. Rev. Lett. **104**, 035003 (2010).
[10]J. W. Berkery, S. A. Sabbagh, H. Reimerdes, R. Betti, B. Hu, R. E. Bell, S. P. Gerhardt, J. Manickam, and M. Podesta, Phys. Plasmas **17**, 082504 (2010).
[11]H. Reimerdes, J. W. Berkery, M. J. Lanctot, A. M. Garofalo, J. M. Hanson, Y. In, M. Okabayashi, S. A. Sabbagh, and E. J. Strait, Phys. Rev. Lett. **106**, 215002 (2011).
[12]I. R. Goumiri, C. W. Rowley, S. A. Sabbagh, D. A. Gates, S. P. Gerhardt, M. D. Boyer, R. Andre, E. Kolemen, and K. Taira, Nucl. Fusion **56**, 036023 (2016).
[13]S. A. Sabbagh, R. E. Bell, J. E. Menard, D. A. Gates, A. C. Sontag, J. M. Bialek, B. P. LeBlanc, F. M. Levinton, K. Tritz, and H. Yuh, Phys. Rev. Lett. **97**, 045004 (2006).
[14]J. E. Menard and NSTX Team, Nucl. Fusion **52**, 083015 (2012).
[15]M. Ono, S. M. Kaye, Y. K. Peng, G. Barnes, W. Blanchard, M. D. Carter, J. Chrzanowski, L. Dudek, R. Ewig, D. Gates, R. E. Hatcher, T. Jarboe, S. C. Jardin, D. Johnson, R. Kaita, M. Kalish, C. E. Kessel, H. W. Kugel, R. Maingi, R. Majeski, J. Manickam, B. McCormack, J. Menard, D. Mueller, B. A. Nelson, B. E. Nelson, C. Neumeyer, G. Oliaro, F. Paoletti, R. Parsells, E. Perry, N. Pomphrey, S. Ramakrishnan, R. Raman, G. Rewoldt, J. Robinson, A. L. Roquemore, P. Ryan, S. Sabbagh, D. Swain, E. J. Synakowski, M. Viola, M. Williams, and J. R. Wilson, Nucl. Fusion **40**, 557 (2000).
[16]J. W. Berkery, S. A. Sabbagh, R. E. Bell, S. P. Gerhardt, B. P. LeBlanc, and J. E. Menard, Nucl. Fusion **55**, 123007 (2015).
[17]J. W. Berkery, S. A. Sabbagh, R. Betti, R. E. Bell, S. P. Gerhardt, B. P. LeBlanc, and H. Yuh, Phys. Rev. Lett. **106**, 075004 (2011).
[18]A. H. Glasser, Phys. Plasmas **23**, 072505 (2016).
[19]J. E. Menard, M. G. Bell, R. E. Bell, D. A. Gates, S. M. Kaye, B. P. LeBlanc, R. Maingi, S. A. Sabbagh, V. Soukhanovskii, and D. Stutman, Phys. Plasmas **11**, 639 (2004).
[20]S. A. Sabbagh, A. C. Sontag, J. M. Bialek, D. A. Gates, A. H. Glasser, J. E. Menard, W. Zhu, M. G. Bell, R. E. Bell, A. Bondeson, C. E. Bush, J. D. Callen, M. S. Chu, C. C. Hegna, S. M. Kaye, L. L. Lao, B. P. LeBlanc, Y. Q. Liu, R. Maingi, D. Mueller, K. C. Shaing, D. Stutman, K. Tritz, and C. Zhang, Nucl. Fusion **46**, 635 (2006).
[21]S. P. Gerhardt, D. A. Gates, S. M. Kaye, R. Maingi, J. E. Menard, S. A. Sabbagh, V. Soukhanovskii, M. G. Bell, R. Bell, J. M. Canik, E. Fredrickson, R. Kaita, E. Kolemen, H. Kugel, B. P. L. Blanc, D. Mastrovito, D. Mueller, and H. Yuh, Nucl. Fusion **51**, 073031 (2011).
[22]S. P. Gerhardt, R. Andre, and J. E. Menard, Nucl. Fusion **52**, 083020 (2012).
[23]J. Manickam, M. S. Chance, S. C. Jardin, C. Kessel, D. Monticello, N. Pomphrey, A. Reiman, C. Wang, and L. E. Zakharov, Phys. Plasmas **1**, 1601 (1994).
[24]V. Igochine, Nucl. Fusion **52**, 074010 (2012).
[25]F. M. Poli, C. E. Kessel, M. S. Chance, S. C. Jardin, and J. Manickam, Nucl. Fusion **52**, 063027 (2012).
[26]J. W. Berkery, R. Betti, S. A. Sabbagh, L. Guazzotto, and J. Manickam, Phys. Plasmas **21**, 112505 (2014).
[27]J. E. Menard, Z. Wang, Y. Liu, R. E. Bell, S. M. Kaye, J. Park, and K. Tritz, Phys. Rev. Lett. **113**, 255002 (2014).
[28]J. Shiraishi, N. Miyato, and G. Matsunaga, Sci. Rep. **6**, 25644 (2016).
[29]J. W. Berkery, R. Betti, and S. A. Sabbagh, Phys. Plasmas **18**, 072501 (2011).
[30]M. Podesta and R. Bell, Rev. Sci. Instrum. **83**, 033503 (2012).
[31]M. Podesta and R. Bell, Plasma Phys. Controlled Fusion **58**, 125016 (2016).
[32]Y. Liu, M. S. Chu, C. G. Gimblett, and R. J. Hastie, Phys. Plasmas **15**, 092505 (2008).
[33]J. W. Berkery, Y. Q. Liu, Z. R. Wang, S. A. Sabbagh, N. C. Logan, J.-K. Park, J. Manickam, and R. Betti, Phys. Plasmas **21**, 052505 (2014).
[34]Y. Liu, I. T. Chapman, M. S. Chu, H. Reimerdes, F. Villone, R. Albanese, G. Ambrosino, A. M. Garofalo, C. G. Gimblett, R. J. Hastie, T. C. Hender, G. L. Jackson, R. J. La Haye, M. Okabayashi, A. Pironti, A. Portone, G. Rubinacci, and E. J. Strait, Phys. Plasmas **16**, 056113 (2009).